Journal of
Materials Chemistry C

PAPER

View Article Online
View Journal | View Issue

Cite this: J. Mater. Chem. C, 2015, 3, 6692

The crucial role of self-assembly in nonlinear optical properties of polymeric composites based on crown-substituted ruthenium phthalocyaninate†

Yulia G. Gorbunova,*[ab] Antonina D. Grishina,[a] Alexander G. Martynov,[a] Tatiyana V. Krivenko,[a] Alexandra A. Isakova,[a] Vladimir V. Savel'ev,[a] Sergey E. Nefedov,[b] Evgeny V. Abkhalimov,[a] Anatoly V. Vannikov[a] and Aslan Yu. Tsivadze[ab]

Received 6th April 2015,
Accepted 18th May 2015

DOI: 10.1039/c5tc00965k

www.rsc.org/MaterialsC

Ruthenium(II) tetra-15-crown-5-phthalocyaninate with axially coordinated molecules of pyrazine [(15C5)$_4$Pc]Ru(pyz)$_2$ (**1**) was synthesized from a carbonyl complex [(15C5)$_4$Pc]Ru(CO)(MeOH) (**2**), and the structure of the solvate complex (**1**)·6CHCl$_3$ was revealed using the single crystal X-ray diffraction method. Analysis of the crystal packing showed that the weak intermolecular interactions, such as CH···π, CH···N, CH···O and CH···Cl, played an essential role in the formation of stable assemblies and their organization within the crystals. The interplay between the intramolecular axial coordinated pyrazine contacts and the weak intermolecular interactions of solvate molecules with crown-ether fragments provided the basis for rationalizing the observed self-assembly of molecules in solutions of tetrachloroethane and polymeric composites with polyvinylcarbazole. The self-assembly was investigated using UV-Vis spectroscopy, dynamic light scattering measurements, atomic force microscopy and transmission electron microscopy techniques. The formation of nanoparticles of complex (**1**) from a tetrachloroethane solution after three cycles of heating to 70 °C/cooling to 5 °C and two days storage was proved. Thin films (7 μm) of polymeric composites with polyvinylcarbazole prepared from a solution containing nanoparticles exhibited a nonlinear optical response measured by the Z-scan technique with application of femtosecond (1030 nm) and nanosecond (1064 nm) pulse lasers. The measured third-order susceptibility ($\chi^{(3)}$) of the polyvinylcarbazole composite with 4 wt% of complex (**1**) was equal to 1.94×10^{-10} esu, while the same composite prepared without the previously described special treatment had zero susceptibility. This result proves the essential role of self-assembly in future development of nonlinear optical materials.

Introduction

Synthesis of compounds with nonlinear optical properties (NLO) is related to the search for the systems that limit the intensity of laser irradiation in nanoseconds and shorter times and thereby protect photosensitive devices and the eye from strong radiation. Among organic components of NLO materials, phthalocyanines (Pcs) constitute one of the most attractive classes of photosensitizers,[1,2] whose strong nonlinearities arise from highly delocalized 18π-electron aromatic systems. Variation of substituents at the periphery of the Pc macrocycle, as well as the metal ion in its cavity and axial ligands, results in a huge family of compounds, thereby allowing the fine tuning of the required physicochemical characteristics. An even larger diversity of properties can be achieved by using a supramolecular assembly of Pc molecules which gives extended aggregates with enhanced nonlinear susceptibility. This effect appears both in solutions of aggregated Pcs[3,4] and in films obtained by various techniques – casting, epitaxial growth, spin-coating, Langmuir–Blodgett, and so on.[3,5–7] To produce such materials, incorporation of Pcs into a polymeric matrix is also widely used.[3,8–10] Formation of such composites typically results in the enhancement of the NLO properties of the Pcs,[11–15] as well as improving their photo- and thermal-stability when they are compared to the same Pc molecules in solution.[10]

Among the substituted Pcs, crown-ether derivatives are very promising building blocks for the assembly of molecules into

[a] Frumkin Institute of Physical Chemistry and Electrochemistry, Russian Academy of Sciences, Leninskiy Pr. 31, Moscow, 119071, Russia. E-mail: yulia@igic.ras.ru
[b] Kurnakov Institute of General and Inorganic Chemistry, Russian Academy of Sciences, Leninskiy Pr. 31, Moscow, 119991, Russia

† Electronic supplementary information (ESI) available: A scheme of the Z-scan measurement technique, molecular structure of complex (**1**), crystal packing of complex (**1**). CCDC 1056316. For ESI and crystallographic data in CIF or other electronic format see DOI: 10.1039/c5tc00965k

cofacial and brick wall supramolecular structures.[16,17] Study of crown-substituted Pcs has attracted attention because of their development, as photorefractive materials, molecular switches and redox-active compounds, as well as sensors for cations and anions and NLO materials.[18–25] It has been established previously that the photoelectric and photorefractive properties of the polymer composites consisting of Ru(II) crown-phthalocyanines with axially coordinated 1,4-diazabicyclo-[2.2.2]octane (DABCO) molecules are enhanced by the formation of supramolecular assemblies.[18,26] The third-order NLO properties of this Ru(II) complex have been measured using Z-scan techniques in a tetrachloroethane (TCE) solution. It has been found that the third-order molecular polarizability per molecule increases by a factor of 3.6 in proceeding from single molecules to the supramolecular assembly formed in solution during the heating–cooling cycles.[27] The morphology of these assemblies was investigated using atomic force microscopy (AFM), which demonstrated the presence of stable supramolecular wires 7–8 nm in height, 100–150 nm in width and 600 nm or more in length.[18] All previous studies of crown-Pc NLO properties have been performed in solution while the NLO behavior in the solid state is also very important for the development of optical devices. It is also known that changing the nature of the axial ligands in metal-Pcs leads to a considerable enhancement in optical limiting response.[9] Taking all these items into consideration, in this paper, the features of self-assembly and the optical behavior of composites of ruthenium(II) tetra-15-crown-5-phthalocyaninate containing axially coordinated molecules of pyrazine $[(15C5)_4Pc]Ru(pyz)_2$ (**1**) with polyvinylcarbazole (PVCZ) measured by the Z-scan technique are reported. The molecular and supramolecular structures of complex (**1**) in the solid state are described using single-crystal X-ray diffraction (XRD) data. The composition and morphology of supramolecular assemblies formed in a TCE solution were studied using transmission electron microscopy (TEM) and AFM, as well as ultraviolet-visible (UV-Vis) spectroscopy and dynamic light scattering (DLS).

Experimental section

Materials

Pyrazine, TCE, methanol (MeOH), *o*-dichlorobenzene (*o*-DCB), PVCZ (glass transition point (T_g) of 200 °C) and trimethylamine *N*-oxide (TMANO; $Me_3NO{\cdot}2H_2O$) were available from commercial suppliers (Acros, Merck, Sigma-Aldrich,). Chloroform ($CHCl_3$; Chimmed, Russia) was stabilized with 0.6–1% ethanol, and then dried over calcium chloride ($CaCl_2$) and distilled over calcium hydride (CaH_2). Neutral alumina (Merck) was used for column chromatography. Phthalocyanine $[(15C5)_4Pc]Ru(CO)(MeOH)$ (**2**) was synthesized using a previously reported method.[28]

Synthesis of bis(pyrazine)(tetra-15-crown-5-phthalocyaninato)-ruthenium(II) (1)

A mixture of $[(15C5)_4Pc]Ru(CO)(MeOH)$ (**2**) (17.4 mg, 12.1 μmol), TMANO (5.4 mg, 48.5 μmol) and 500 mg of pyrazine in 3 ml of $CHCl_3$ was refluxed for 1 h until the Q-band of carbonyl the complex (655 nm) vanished in the UV-Vis spectrum of a sample of the reaction mixture. After cooling to room temperature, the mixture was poured into hexane (50 ml), and the resulting dark blue precipitate was filtered off and chromatographed on neutral alumina. Elution with $CHCl_3$ + 0–2 vol% MeOH gave 16.8 mg (~90%) of a mixture containing the target complex $[(15C5)_4Pc]Ru(pyz)_2$ (**1**) together with 15 mol% of the heteroligand complex $[(15C5)_4Pc]Ru(pyz)(Me_3N)$ (**1a**) as shown by proton-nuclear magnetic resonance (^{1}H-NMR). To remove the side product, the mixture of complexes was dissolved in 3 ml of *o*-DCB, 125 mg of pyrazine was added, and the solution was refluxed for 15 min under a slow argon flow. After cooling to room temperature, the mixture was poured into hexane (50 ml), and the dark blue precipitate was filtered and dried. The NMR investigation of this precipitate showed that there was complete substitution of axially coordinated trimethylamine with pyrazine.

^{1}H-NMR [600 MHz, deuterated chloroform ($CDCl_3$)] δ, ppm: 8.59 (s, 8H, H_{Pc}), 6.46 (d, J = 4.5 Hz, 4H, *m*-Pyz), 4.69 (m, 16H, α-OCH_2), 4.17 (m, 16H, β-OCH_2), 3.90 (m, 32H, γ, δ-OCH_2), 2.38 (d, J = 4.5 Hz, 4H, *o*-Pyz). UV-Vis (λ_{max}, nm ($\lg\varepsilon$)): 631 (4.79) 576 sh. 362 (4.54) 322 (5.15), infrared (IR) (ν, cm^{-1}): 2867 (w), 1606 (w), 1583 (m), 1445 (m), 1471 (m), 1447 (m), 1399 (m), 1373 (m), 1227 (vs), 1201 (m), 1148 (m), 1109 (vs), 1066 (s), 979 (vs), 936 (s), 906 (m), 860 (m), 817 (s), 735 (s); high resolution mass spectroscopy with electrospray ionization (HR-ESI-MS) calculated for $C_{72}H_{81}N_{12}NaO_{20}Ru$ $[M + H + Na]^{2+}$ 779.232; found 779.230.

Characterization

NMR spectra were recorded on a Bruker Avance 600 MHz spectrometer. The residual proton signals of the deuterated solvent were used as the reference for the NMR spectra.[29] UV-Vis spectra were measured with Varian Cary-100 and Shimadzu UV-3101PC spectrophotometers in quartz cells with a 10 mm optical path. A Thermo Nicolet Fourier-transform Nexus spectrometer with a Pike Technologies micro-ATR accessory was used to record IR spectra. Accurate mass measurements (HR-ESI-MS) were performed on a Bruker maXis impact mass spectrometer. Solutions of the target compound in $CHCl_3$/MeOH (1 : 1) were used for the analysis. Samples for AFM were prepared by casting 5 μl of a 7×10^{-4} M solution in TCE onto a freshly peeled mica surface. The AFM investigation was carried out using a Bruker EnviroScope AFM with a NanoScope V controller. Image acquisition was performed in the tapping mode. NT-MDT Corporation cantilevers (Moscow, Russia) NSG 01 resonance frequency 150 kHz, force constant 5.5 N m^{-1}, curvature radius 10 nm, were used. Data were processed using WSxM 4.11 software (Nanotec Electronica, Madrid, Spain).[30]

Transmission electron microscopy (TEM) images and selected area electron diffraction patterns were obtained using a Carl Zeiss LEO912 AB OMEGA TEM instrument operating at 100 kV. Before analysis by TEM, the solution of complex (**1**) was dripped onto a carbon-coated copper grid and air-dried at room temperature.

The size of nanoparticles in the solution was determined using a DLS technique. Prior to the measurements, solutions

were thermostated at 20 °C. The measurements were carried out in a quartz cell on a Delsa Nano C particle analyzer (Beckman Coulter, USA) at a wavelength of 658 nm using the Delsa Nano v.3.73 software package. The average particle sizes were obtained from particle size distributions calculated using the autocorrelation functions of scattering intensity by the CONTIN method.

X-ray structure analysis

Dark blue crystals of solvate $[(15C5)_4Pc]Ru(pyz)_2\cdot 6CHCl_3$ were obtained by slow evaporation of its solution in $CHCl_3$. Single-crystal XRD experiments were carried out using a Bruker SMART APEX II diffractometer with a charge coupled device area detector (graphite monochromator, Mo-Kα radiation, λ = 0.71073 Å, ω-scans). a = 12.3589(11) Å, b = 14.0410(12) Å, c = 14.1355(12) Å, α = 96.287(2)°, β = 104.6120(10)°, γ = 102.610(2)°, V = 2280.9(3) Å^3 (150 K), Z = 1, D_{calc} = 1.639 g cm^{-3}, 25 204 measured reflections, 12 016 [R(int) = 0.0774] independent reflections with $F^2 > 2\sigma(I)$, μ = 0.479 cm^{-1}, R_1 = 0.0710, wR_2 = 0.1519. The semi-empirical Bruker/Siemens area detector absorption (SADABS)[31] method was applied for absorption correction. The structures were solved using direct methods and refined using the full-matrix least-squares technique on F^2 with anisotropic displacement parameters for all non-hydrogen atoms. All the hydrogen atoms in the complexes were placed geometrically and included in the structure factor calculation in the riding motion approximation. All the data reduction and further calculations were performed using the SAINT[32] and SHELXTL-97[33] program packages. CCDC 1056316.

Composite fabrication and Z-scan measurements

A solution of complex (**1**) in TCE (c = 7 × 10^{-4} mol L^{-1}) was heated to 70 °C and cooled to 5 °C with simultaneous measurements of UV-Vis spectra in the 400–1400 nm range. Heating–cooling cycles were repeated three times. For preparation of polymeric composites, PVCZ (Aldrich, M_W = 1.1 × 10^6, T_g = 200 °C) was added to the thermally treated and aged for 48 h solution (4 wt% of complex (**1**)), and the mixture was agitated with a magnetic stirrer. The viscous solution obtained was poured onto a polyethylene transparent film fixed in a frame and dried on a heating plate. After evaporation of the solvent, the thickness of the composite was measured with an interferometer: the thickness of the layer was 7 μm. NLO characteristics were determined using the Z-scan technique with an OneFive Origami-10 femtosecond laser (1030 nm) and a Nd:YAG nanosecond pulse laser (1064 nm). The pulse length of the femtosecond laser was 217 fs with a rate of 74.82 × 10^6 s^{-1} and an average laser light power of 0.15 J s^{-1}. The energy of light per pulse was 2 × 10^3 J with total power I = 0.15/(74.82 × 10^6 × 217 × 10^{-15}) = 9.24 × 10^3 W. The diameter of the laser beam at the focal point was 20.6 μm, and the light intensity at the lens focal point was $I_0 = I/(\pi w_0^2)$ = 6.92 × 10^8 W cm^{-2}. The femtosecond laser beam was opened for ~470 μs and the rise time of the signal in the initial period was about 10 μs. Measurements were carried out by irradiation of the sample for 40 μs and 450 μs. The nanosecond laser emits a train of five 10 ns pulses with a total intensity of 0.75 W. A holder with the polymeric composite was moved along the beam direction from the range of $-z$ to $+z$. The light transmittance through the sample was measured in two modes, namely, closed aperture transmittance (T_{CA}) or open aperture transmittance (T_{OA}) (Fig. S1, ESI†).

Results and discussion

Synthesis

Ru(II) tetra-15-crown-5-phthalocyaninate with axially coordinated pyrazine molecules, $[(15C5)_4Pc]Ru(pyz)_2$ (**1**), was synthesized using the previously described carbonyl complex $[(15C5)_4Pc]$-Ru(CO)(MeOH) (**2**).[28] Complex (**2**) was treated with TMANO in the presence of excess pyrazine in refluxing $CHCl_3$.[34] This resulted in the formation of a mixture of two decarbonylated complexes – target complex (**1**) and a side product with axially coordinated pyrazine and trimethylamine ligands $[(15C5)_4Pc]$-Ru(pyz)(NMe$_3$) (**1a**) in a 85/15 ratio as shown by NMR (Scheme 1). To avoid tedious chromatographic separation of these complexes, this mixture was refluxed in *o*-DCB in the presence of excess pyrazine. Because of the high boiling point of *o*-DCB (180 °C), volatile trimethylamine was removed from the Ru(II) coordination sphere and was replaced with pyrazine, giving a pure target complex (**1**).

X-ray diffraction analysis

Single crystals of complex (**1**) suitable for XRD analysis were obtained by slow evaporation of a solution of the complex in $CHCl_3$.

It was found that, in the centrosymmetric molecule, the Ru(II) atom has an octahedral environment formed by four isoindole nitrogen atoms belonging to the phthalocyanine macrocycle [the Ru–N$_{iso}$ distances were 1.984(4)–1.999(4) Å] and two nitrogen atoms from the coordinated pyrazine molecules [Ru–N$_{pyz}$ = 2.089(4) Å] (Fig. 1, Fig. S2, ESI†). Both pyrazine molecules are located in the same plane that includes *meso*-nitrogen atoms line N(4)/N(4A) and the ruthenium atom. This plane is almost orthogonal to the phthalocyanine plane [tilt angle is 5.1°]. This arrangement of pyrazine molecules might be caused by formation of relatively short intramolecular hydrogen bonds and CH···π contacts of carbons atoms C(33) and C(36) with carbon and nitrogen atoms of the six member cycle of phthalocyanine Ru–N(1A)–C(32)–N(4)–C(31)–N(3) [C···C contacts are 3.382–3.480 Å; N···C contacts are 3.093–3.211 Å]. However, such geometry can be caused by the intermolecular CH···O contacts of these atoms as well as carbon atoms C(34) and C(35) with oxygen atoms O(3) and O(8) of the crown ether substituents of the other complex (**1**) located in the crystal cell [C···O contacts are 3.174–3.337 Å] (Fig. 1 and Fig. S3, ESI†).

Notably, the Ru–N$_{pyz}$ distance is significantly shorter than the one observed in the similar crystal structure of $[(15C5)_4Pc]$-Ru(DABCO)$_2$ reported previously[35] [Ru–N$_{DABCO}$ = 2.244(3) Å], suggesting stronger binding of the aromatic ligand in comparison with the aliphatic amine. Apparently, this stronger binding

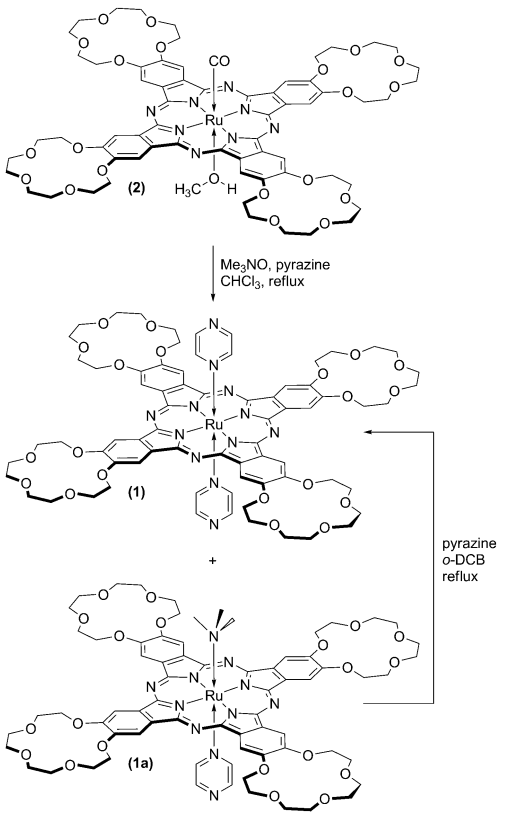

Scheme 1

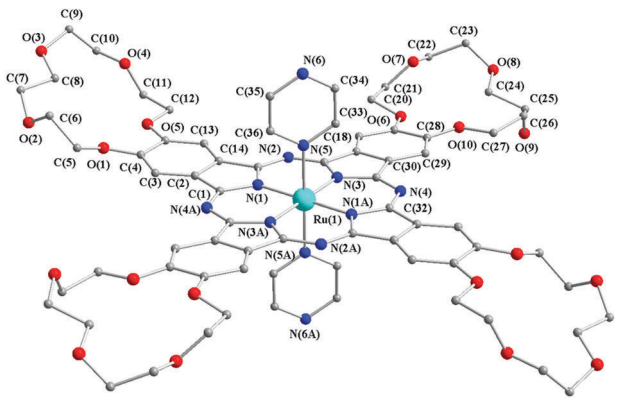

Fig. 1 Molecular structure of complex (**1**). Hydrogen atoms are omitted for clarity.

is a reason for the successful substitution of the NMe_3 ligand with pyrazine at an elevated temperature.

The molecules of the complex form a brick wall similar to three-dimensional packing where the planes of all the phthalocyanine macrocycles are parallel to each other (Fig. S3, ESI†). Each molecule of the complex is surrounded by eight other molecules. Such packing is the result of weak but multiple intermolecular interactions dominated by contacts with crown-ether macrocycles. Their oxygen atoms form CH···O contacts with the pyrazine moiety as described previously. In addition, OCH_2 moieties are involved in the formation of weak intermolecular hydrogen bonds with pyrazine nitrogen atoms and phthalocyanine *meso*-N atoms. Finally, multiple CH···π contacts are formed by the OCH_2 groups and benzene moieties of the phthalocyanine ring. It should be mentioned that pyrazine molecules do not form stacking contacts with each other or with other π-systems.

The voids between the molecules are filled with $CHCl_3$ molecules, therefore forming the (**1**)·6$CHCl_3$ solvate. Notably, four chloroform molecules form hydrogen bonds with only one of the oxygen atoms of the crown-ether macrocycle [C(37)···O(2) 3.126; C(38)···O(4) 3.134 (Fig. 2)], in contrast to the crystal lattice of $[(15C5)_4Pc]Ru(DABCO)_2 \cdot 7CHCl_3$ or the sandwich lanthanide complexes where at least four oxygen atoms of crown ethers are involved in binding with $CHCl_3$.[35–37] This might be explained by numerous weak CH···Cl contacts of $CHCl_3$ molecules with phthalocyanine aromatic protons. Solvate $CHCl_3$ forms clusters constructed of six molecules combined through the Cl···Cl contacts [3.42–3.47 Å].[38]

Thus, the X-ray data obtained have demonstrated that possible multiple weak intermolecular interactions within the crown-ether substituted phthalocyanines are playing a key role not only in single crystal growth but that, in general, such interactions are responsible for the complex geometry as well as the crystal packing of molecules.

Assembly in solution and thin films

The measurements of UV-Vis spectra of (**1**) dissolved in TCE after the heating and cooling procedure were taken with a spectrophotometer equipped with a Peltier cell. Being in the monomeric state, complex (**1**) revealed a single Q-band at 634 nm in the UV-Vis spectrum of the solution (Fig. 3). After three cycles of heating this solution to 70 °C and slow cooling to 5 °C, the Q-band was broadened with a simultaneous decrease in intensity, which corresponds to aggregation of the molecules. A similar behavior was observed previously for other crown-phthalocyaninates.[16,17]

The simultaneous DLS measurements after the first heating–cooling cycle revealed the formation of nanoparticles with an average size of 1.5 ± 0.4 nm (Fig. 4), which were absent in the fresh solution. One more heating–cooling cycle resulted in further aggregation of complex (**1**), which was followed by a decrease in intensity of the Q-band (Fig. 3), as well as in negligible growth of the nanoparticle size. The third heating–cooling cycle did not result in dramatic changes of the UV-Vis spectra or the size of the nanoparticles, suggesting that the formation of nanoparticles was essentially finished during the second heating–cooling cycle. Notably, the colloidal system obtained was unstable, and the size of nanoparticles continued to grow with time during the storage of the solution. Thus, the DLS profile after the storage of the thermally treated solution for 12 h at room temperature indicated that such aging of the sample gives rise to spontaneous self-assembly of molecules with the formation of 50.4 ± 17.6 nm particles and after storage for 48 h, the solution contains particles with the average size of 213 ± 55.2 nm (Fig. 4). It should be noted that similar storage of a thermally untreated solution did not lead to the formation of

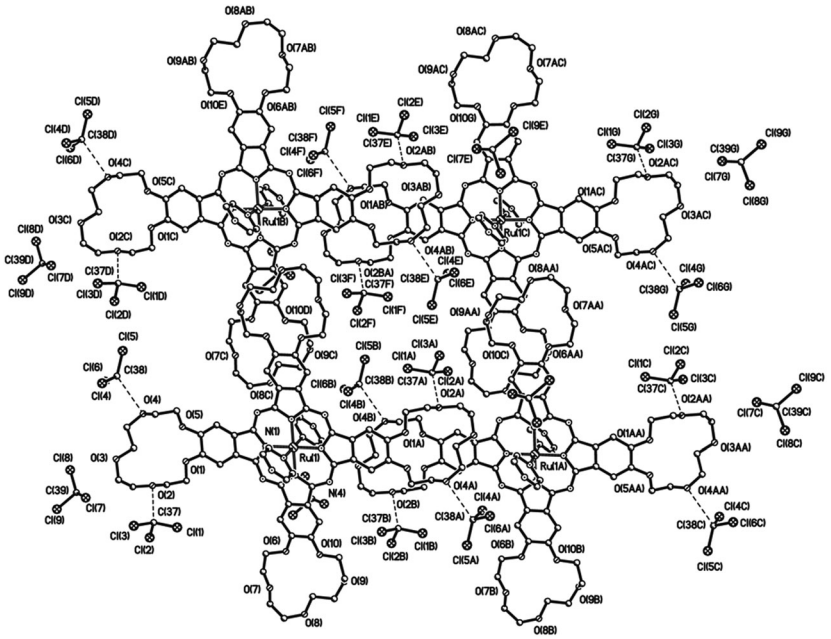

Fig. 2 Crystal packing of (**1**)·6$CHCl_3$ solvate. Hydrogen atoms are omitted for clarity.

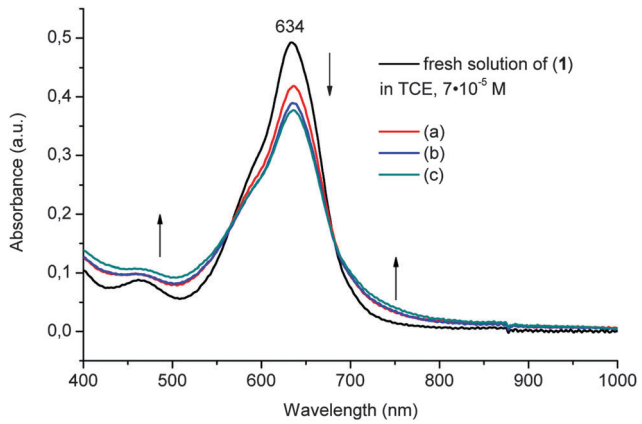

Fig. 3 Q-band region of UV-Vis spectra of a solution of (**1**) in TCE before and after the first (a), second (b) and third (c) cycle of heating to 70 °C and cooling to 5 °C.

such assemblies. Therefore, simultaneous application of UV-Vis spectroscopy and DLS measurements demonstrates the formation of supramolecular assemblies by (**1**) in TCE solutions after the previous thermal treatment and further storage of this solution.

The investigation of the assembling of molecules in thin solid films is also very important for finding out the peculiarities of the complex behavior during the composite preparation. For this purpose, the morphology of cast films obtained from a freshly prepared solution of complex (**1**) and from thermally treated solutions was studied using AFM and TEM. Fig. 5 demonstrates the images of $[(15C5)_4Pc]Ru(pyz)_2$ cast films on the mica surface. AFM studies of the cast film obtained from a freshly prepared solution of complex (**1**) on mica did not reveal the formation of large particles. Instead, cylindrical particles of approximately 10 nm in height were observed (Fig. 5a–c). However, when a solution of complex (**1**) in TCE was heated and cooled three times and cast on the mica surface, the formation of large cubic aggregates was observed by AFM (Fig. 5d–f). The average size of these aggregates was 400 × 200 nm. Taking into consideration the single-crystal XRD data, it can be assumed that molecules of TCE take part in the self-assembly of molecules (**1**) to give brick wall structures.

Furthermore, the formation of such assemblies results in the appearance of an electron diffraction pattern with strong reflections in the TEM images, which is evidence of their crystalline nature (Fig. 6). It should be noted that the cast film prepared for TEM from a fresh solution did not give rise to electron diffraction because of the amorphous nature of the particles.

Finally, in order to understand the assembly behavior of complex (**1**) in the polymeric composite, the UV-Vis spectra of the PVCZ composite with (**1**) (4 wt%) were investigated. Fig. 7a shows the spectrum of the PVCZ–(**1**) composite prepared from a fresh solution in TCE. The typical broadening of the Q-band of a solid sample in the comparison with that of a solution occurs without any shift of the band. In contrast, when a film is prepared from a thermally treated solution, the red shift of the Q-band with additional absorption up to 1400 nm occurs, which correlates with the formation of brick wall assemblies of the phthalocyanines (Fig. 7b).[39,40] It was shown earlier that such assemblies in polymeric composites were responsible for the photorefractive properties of ruthenium phthalocyanine in near-IR spectral range.[26,27]

Z-scan measurement of the optical nonlinearity of composites

At the high intensity of laser irradiation in the Rayleigh range, the volume polarization of the sample $P(E)$ contributed

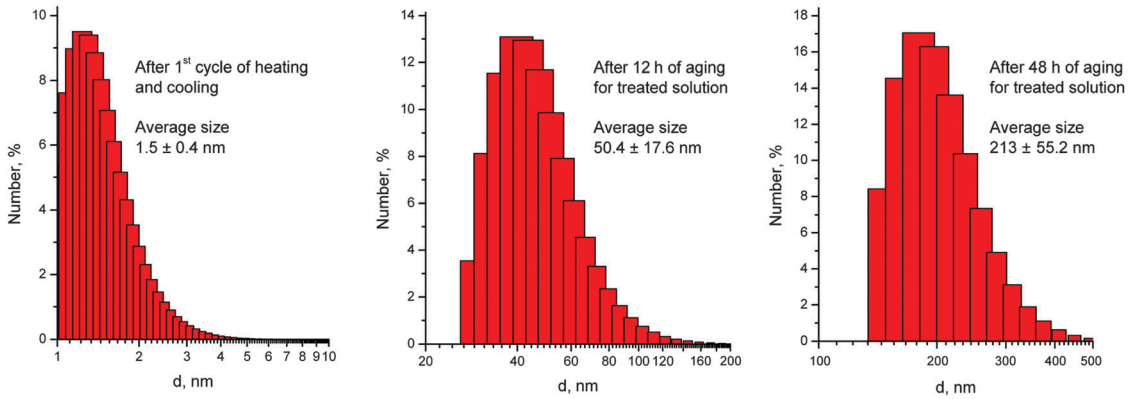

Fig. 4 Histograms of particle size distributions of 7×10^{-5} M complex (**1**) in TCE solution, obtained by DLS.

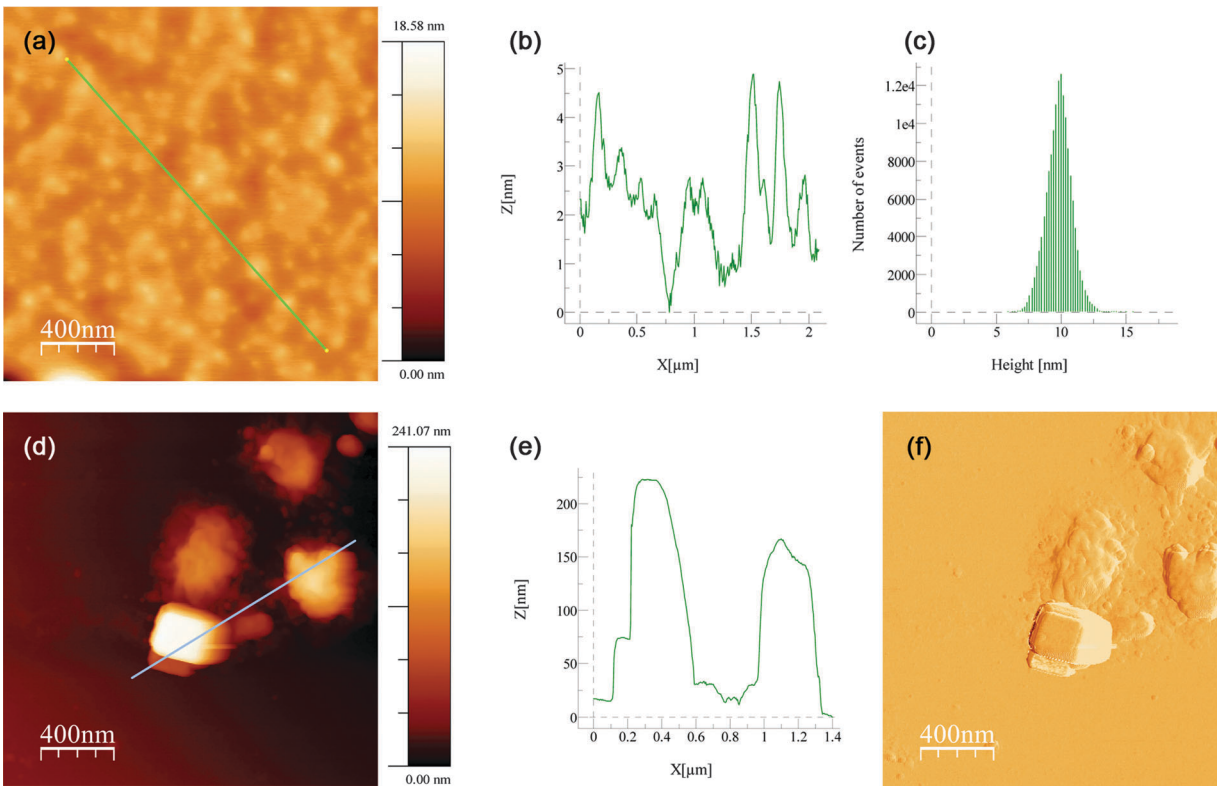

Fig. 5 AFM images of complex (**1**): (a) cast film prepared from a fresh solution (7×10^{-4} M); (b) line profile showing the size of the particles; (c) histogram showing the height of the particles; (d) cast film prepared from the thermally treated solution (3 cycles); (e) line profile showing the size of the crystals; (f) phase image of the crystals.

significantly to the nonlinear components. In a solution or polymeric film at random centrosymmetric orientation of nonlinear chromophores, the second-order susceptibility vanishes to zero and $P(E) = \chi^{(1)}E + \chi^{(3)}E^3$ (where E is the electric field of an electromagnetic wave, $\chi^{(1)}$ is the linear susceptibility and $\chi^{(3)}$ is the third-order susceptibility).

As $n^2 = 1 + 4\pi P/E$, hence in eqn (1):

$$\begin{aligned} n &= (1 + 4\pi\chi^{(1)})^{0.5} \times \{1 + [4\pi\chi^{(3)}E^2/(1 + 4\pi\chi^{(1)})]\}^{0.5} \\ &= (1 + 4\pi\chi^{(1)})^{0.5} \times \{1 + [2\pi\chi^{(3)}E^2/(1 + 4\pi\chi^{(1)})]\} \\ &= n_0 + (2\pi\chi^{(3)}E^2/n_0), \text{ or } n = n_0 + n_2I_0, \end{aligned} \quad (1)$$

where $n_0 = (1 + 4\pi\chi^{(1)})^{0.5}$ is the refractive index at low light intensity (for TCE and PVCZ $n_0 = 1, 5$); n_2I_0 is the contribution of the third-order nonlinearity at the laser irradiation with intensity I_0 at $z = 0$. According to eqn (1), the refractive index increases or decreases depending on the n_2 sign. The optical absorption at $z = 0$ increases and includes the linear (α_0) and nonlinear (β) terms:

$$\alpha = \alpha_0 + \beta I_0 \quad (2)$$

The nonlinear characteristics n_2I_0 and βI_0 were evaluated from the dependence of light transmission on the distance

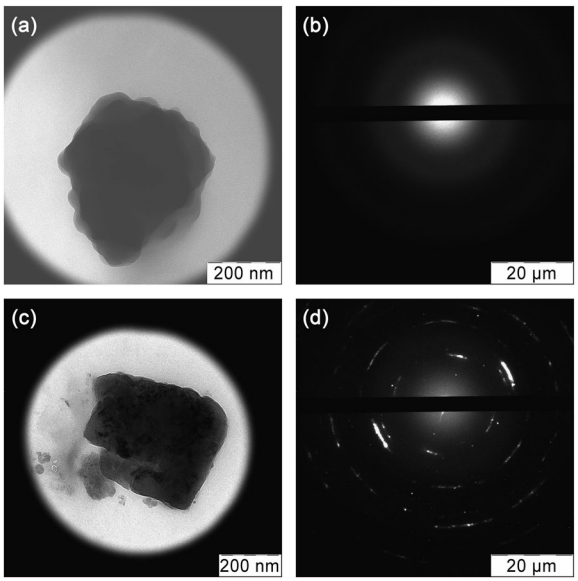

Fig. 6 TEM images of complex (**1**): (a) cast film prepared from a fresh solution (7×10^{-4} M) on a graphite surface; (b) electron diffraction pattern from the film (a); (c) cast film prepared from a thermally treated solution on a graphite surface; (d) electron diffraction pattern from the film (c).

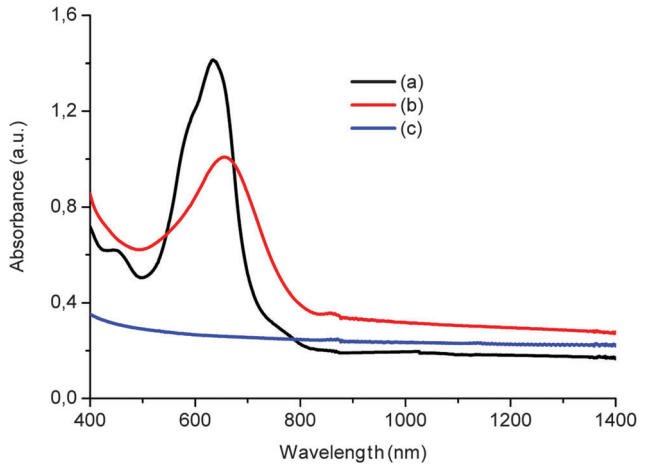

Fig. 7 UV-Vis spectra of the PVCZ composite with complex (**1**) (4 wt%). The 7 μm thick film was prepared from a fresh solution of complex (**1**) in TCE (a) and from a solution subjected to three cycles of heating to 70 °C and slow cooling to 5 °C (b); UV-Vis spectra of a PVCZ film without the complex (c).

from the focal point. When n_2 has a positive value, the sample acts as the additional focusing lens (Fig. S1, ESI†). When the sample is located in the $-z$ range, the beam diameter in the aperture zone increases, which results in a decrease in the beam light portion transmitted through the aperture to the photodetector. When the sample is moved to the $+z$ range, an additional focusing of light by the sample leads to a decrease in the beam diameter in the aperture plane and, thus, to an increase in the beam portion transmitted through the aperture. Therefore, Z-scan T_{CA} curves recorded by a photodetector have a minimum in the pre-focal domain and a maximum in the post-focal domain. Fig. 8a shows the T_{CA} dependence on the distance to the focal point ($z = 0$) for composites of (**1**) with PVCZ [4 wt% of complex (**1**)] prepared from a fresh solution of complex (**1**) in TCE and subjected to three cycles of heating to 70 °C and slow cooling to 5 °C with further aging for 48 h. It should be noted that the nonlinear response arises only after cyclic thermal treatment of the solution in TCE. Experimental values were approximated by the following theoretical dependence:[41,42]

$$T_{CA} = 1 - 4\Delta\Phi_0 x/[(x^2 + 1)(x^2 + 9)] \quad (3)$$

Here, $x = z/z_0$ is the relative distance from the cell to the focal point; $z_0 = n_0\pi w_0^2/\lambda$ is the Rayleigh range, which is known to correspond to the distance from the focal point to the position where the beam radius equals $w_0 \times (2)^{0.5}$; and w_0 is the beam radius at the lens focal point. The approximation was made by fitting $\Delta\Phi_0$ and w_0 parameters. The best fit (solid line in Fig. 8a) corresponds to the theoretical curve 1 at $\Delta\Phi_0 = 0.1$ and $w_0 = 20.6$ μm.

The imaginary part of the susceptibility can be found from the open aperture transmittance (T_{OA}).

Fig. 8b shows the $T_{OA} - z$ dependence, where experimental data are approximated with the following theoretical expression (solid line):[41,42]

$$T_{OA} = [\ln(1 + q_0/(1 + x^2))]/[q_0/(1 + x^2)] \quad (4)$$

According to the known equations:

$$n_2 I_0 = \Delta\Phi_0\lambda/2\pi L_{eff} \quad (5)$$

$$\beta I_0 = q_0/L_{eff} \quad (6)$$

$n_2 I_0 = 0.002$ (when $L_{eff} = 7$ μm). The value of I_0 under these conditions is 6.92×10^8 W cm^{-2}, therefore, $n_2 = 3.4 \times 10^{-12}$. The real part of the third-order susceptibility is related to n_2 by the formula: $\chi^{(3)} = n_2 \times (n_0^2/0.0394)$. When n_0 is 1.5 (TCE, PVCZ), $\chi^{(3)} = 1.93 \times 10^{-10}$ esu.

The imaginary part of the susceptibility found from the open aperture transmittance experiment (Fig. 8b) corresponds to the best approximation when $q_0 = 0.012$ and parameter β calculated from eqn (6) is 2.5×10^{-8}. The imaginary part of the third-order susceptibility is related to factor β by the formula: $\chi^{(3)} = (\beta\lambda/4\pi) \times (n_0^2/0.0394)$ and its value corresponds to: $\chi^{(3)} = 1.2 \times 10^{-11}$ esu.

Thus, the total third-order susceptibility is determined by the real part and is equal to: $\chi^{(3)} = \{[\mathrm{Re}\,\chi^{(3)}]^2 + [\mathrm{Im}\,\chi^{(3)}]^2\}^{0.5} = 1.94 \times 10^{-10}$ esu.

The T_{OA}–z dependences were also measured in the nanosecond range. Fig. 9 shows the dependence of the relative quenching of the laser beam on the incident energy at $z = 0$ measured in samples prepared from a fresh solution of complex (**1**) in TCE, as well as from solutions subjected to three cycles of heating to 70 °C and slow cooling to 5 °C.

A decrease in the optical transmission of the sample at high incident energies is observed. Although the value of this decrease is not very high (only 0.82 at an incident energy of about 4000 J cm^{-2}), this observation reveals the prospects of the

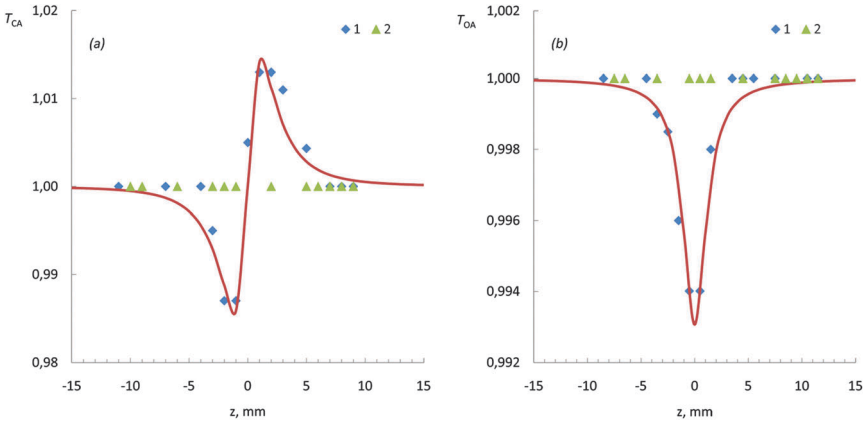

Fig. 8 Z-scan curves measured with (a) closed aperture and (b) open aperture using a femtosecond laser. Samples were prepared from a solution of (**1**) in TCE subjected to three cycles of heating to 70 °C and slow cooling to 5 °C (**1**) and from a fresh solution (**2**). Composites contain PVCZ and complex (**1**) (4 wt%).

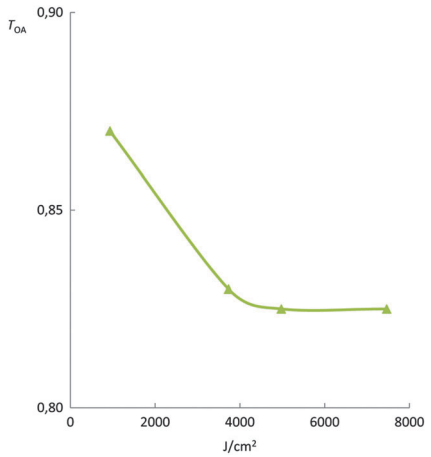

Fig. 9 Dependence of optical transmission with open aperture (T_{OA}) on the incident energy at z = 0 measured in samples prepared from a solution subjected to three cycles of heating to 70 °C and slow cooling to 5 °C.

further application of the proposed methodology for fabrication of NLO supramolecular materials containing well-defined crystalline nanoparticles constructed from crown phthalocyaninates and incorporated into polymeric matrixes.

Conclusions

The detailed investigation of the structure and the optical behavior of Ru(II) tetra-15-crown-5-phthalocyaninate containing axially coordinated molecules of pyrazine was carried out. The features of self-assembly of complex in TCE solution, thin films and polymeric composites with polyvinylcarbazole were revealed. It was found that the nonlinear response of composites arises only after cyclic thermal treatment of the solution in tetrachloroethane and storage for up to 48 h. At the same time, it has been demonstrated that the crystal lattice of Ru(II) crown-phthalocyaninate contains numerous weak contacts (CH···π, CH···N, CH···O, CH···Cl), which are responsible for the formation of nanoparticles in high boiling point solvents, as well as in polymeric films. Anisotropy of the optical properties of these compounds is determined by the architecture of the ensembles and nanoparticles, whose size and geometry depend on the number and duration of heating–cooling cycles as well as aging time. Thus, it confirms that self-assembly has an essential effect on the nonlinear optical behavior of the ruthenium phthalocyaninate polymeric composites.

It is expected that the developed methodology can be used for preparation of novel efficient composite optical limiters starting from other crown phthalocyaninates. Among them there might be trivalent metal tetra-15-crown-5-phthalocyaninates, whose nonlinear optical properties have been previously investigated only in TCE solution. For example, it was shown that gallium(III) or yttrium(III) tetra-15-crown-5-phthalocyaninates have the values: $\chi^{(3)} = (3 \pm 1) \times 10^{-10}$ esu[20,25] whereas that of indium(III) tetra-15-crown-5-phthalocyaninate had an increased $\chi^{(3)}$ value of up to 13.4×10^{-10} esu.[21] However, thermally induced self-assembly in solution of these complexes followed by fabrication of polymeric composites has not been studied and its influence on their nonlinear optical properties would be the subject of further investigations.

Acknowledgements

We gratefully acknowledge support from the Russian Foundation for Basic Research (Project no. 14-03-00049_a and 14-03-00977_a) and OPTEC LLC (Contract No. 49/2014/75-Msk). The authors are grateful to Dr S. S. Abramchuk (INEOS RAS) for help with the TEM experiments.

Notes and references

1 G. de la Torre, P. Vazquez, F. Agullo-Lopez and T. Torres, *Chem. Rev.*, 2004, **104**, 3723–3750.
2 M. Calvete, G. Y. Yang and M. Hanack, *Synth. Met.*, 2004, **141**, 231–243.
3 M. Nicolau, G. Rojo, T. Torres and F. Agulló-López, *J. Porphyrins Phthalocyanines*, 1999, **3**, 703–711.

4 L. Yang, Z. Chen, S. Zhang, L. Niu, C. Tung, Y. Chi, J. Xiang and F. Zhang, *Dyes Pigm.*, 2014, **102**, 251–256.
5 M. K. Casstevens, M. Samoc, J. Pfleger and P. N. Prasad, *J. Chem. Phys.*, 1990, **92**, 2019–2024.
6 J. M. Fox, T. J. Katz, S. Van Elshocht, T. Verbiest, M. Kauranen, A. Persoons, T. Thongpanchang, T. Krauss and L. Brus, *J. Am. Chem. Soc.*, 1999, **121**, 3453–3459.
7 S. Fang, H. Tada and S. Mashiko, *Appl. Phys. Lett.*, 1996, **69**, 767–769.
8 J. J. Doyle, J. Wang, S. M. O'Flaherty, Y. Chen, A. Slodek, T. Hegarty, L. E. Carpenter II, D. Wöhrle, M. Hanack and W. J. Blau, *J. Opt. A: Pure Appl. Opt.*, 2008, **10**, 075101.
9 S. Tekin, U. Kürüm, M. Durmuş, H. G. Yaglioglu, T. Nyokong and A. Elmali, *Opt. Commun.*, 2010, **283**, 4749–4753.
10 J. Britton, C. Litwinski, E. Antunes, M. Durmuş, V. Chaukea and T. Nyokong, *J. Macromol. Sci., Part A: Pure Appl.Chem.*, 2013, **50**, 110–120.
11 M. Yüksek, A. Elmali, M. Durmuş, H. Gul Yaglioglu, H. Ünver and T. Nyokong, *J. Opt.*, 2009, **12**, 015208.
12 J. Britton, M. Durmuş, V. Chauke and T. Nyokong, *J. Mol. Struct.*, 2013, **1054–1055**, 209–214.
13 C. Mkhize, J. Britton and T. Nyokong, *Polyhedron*, 2014, **81**, 607–613.
14 K. E. Sekhosana, E. Amuhaya and T. Nyokong, *Polyhedron*, 2015, **85**, 347–354.
15 K. Sanusi and T. Nyokong, *J. Photochem. Photobiol., A*, 2015, **303–304**, 44–52.
16 Y. G. Gorbunova, A. G. Martynov and A. Y. Tsivadze, in *Handbook of Porphyrin Science*, ed. K. M. Kadish, K. M. Smith and R. Guilard, World Scientific Publishing, 2012, vol. 24, pp. 271–388.
17 A. G. Martynov, Y. G. Gorbunova and A. Y. Tsivadze, *Russ. J. Inorg. Chem.*, 2014, **59**, 1627–1656.
18 A. D. Grishina, Y. G. Gorbunova, V. I. Zolotarevsky, L. Y. Pereshivko, Y. Y. Enakieva, T. V. Krivenko, V. Savelyev, A. V. Vannikov and A. Y. Tsivadze, *J. Porphyrins Phthalocyanines*, 2009, **13**, 92–98.
19 A. V. Vannikov, Y. G. Gorbunova, A. D. Grishina and A. Y. Tsivadze, *Prot. Met.*, 2013, **49**, 57–65.
20 A. V. Vannikov, A. D. Grishina, Y. G. Gorbunova, T. V. Krivenko, A. S. Laryushkin, L. A. Lapkina, V. Savelyev and A. Y. Tsivadze, *J. Polym. Sci., Part A: Polym. Chem.*, 2011, **53**, 1069–1075.
21 A. D. Grishina, Y. G. Gorbunova, T. V. Krivenko, L. A. Lapkina, V. V. Savel'ev, A. V. Vannikov and A. Y. Tsivadze, *Prot. Met.*, 2014, **50**, 472–479.
22 S. L. Selektor, V. V. Arslanov, Y. G. Gorbunova, O. A. Raitman, L. S. Sheinina, K. P. Birin and A. Y. Tsivadze, *J. Porphyrins Phthalocyanines*, 2008, **12**, 1154–1162.
23 S. L. Selektor, A. V. Shokurov, V. V. Arslanov, Y. G. Gorbunova, K. P. Birin, O. A. Raitman, F. Morote, T. Cohen-Bouhacina, C. Grauby-Heywang and A. Y. Tsivadze, *J. Phys. Chem. C*, 2014, **118**, 4250–4258.
24 L. A. Lapkina, N. Y. Konstantinov, V. E. Larchenko, Y. G. Gorbunova and A. Y. Tsivadze, *J. Porphyrins Phthalocyanines*, 2009, **13**, 859–864.
25 A. V. Vannikov, A. D. Grishina, Y. G. Gorbunova, V. I. Zolotarevskii, T. V. Krivenko, A. S. Laryushkin, L. A. Lapkina, V. V. Savel'ev and A. Y. Tsivadze, *High Energy Chem.*, 2015, **49**, 36–43.
26 A. D. Grishina, F. Y. Konnov, Y. G. Gorbunova, Y. Y. Enakieva, L. Y. Pereshivko, T. V. Krivenko, V. Savelyev, A. V. Vannikov and A. Y. Tsivadze, *Russ. J. Phys. Chem. A*, 2007, **81**, 982–989.
27 A. D. Grishina, Y. G. Gorbunova, Y. Y. Enakieva, T. V. Krivenko, V. Savelyev, A. V. Vannikov and A. Y. Tsivadze, *High Energy Chem.*, 2008, **42**, 297–304.
28 Y. Y. Enakieva, Y. G. Gorbunova, S. G. Sakharov and A. Y. Tsivadze, *Russ. J. Inorg. Chem.*, 2002, **47**, 1815–1820.
29 G. R. Fulmer, A. J. M. Miller, N. H. Sherden, H. E. Gottlieb, A. Nudelman, B. M. Stoltz, J. E. Bercaw and K. I. Goldberg, *Organometallics*, 2010, **29**, 2176–2179.
30 I. Horcas, R. Fernández, J. M. Gómez-Rodríguez, J. Colchero, J. Gómez-Herrero and a. M. Baro, *Rev. Sci. Instrum.*, 2007, **78**, 013705.
31 G. M. Sheldrick, *SADABS*, Bruker AXS Inc., Madison, WI-53719, USA, 1997.
32 *SMART V5.051 and SAINT V5.00, Area detector control and integration software, Bruker AXS Inc., Madison, WI-53719, USA, 1998.*, Bruker AXS Inc., Madison, WI-53719, USA, 1998.
33 G. M. Sheldrick, *SHELXTL-97 V5.10*, Bruker AXS Inc., Madison, WI-53719, USA, 1997.
34 Y. G. Gorbunova, Y. Y. Enakieva, S. G. Sakharov and A. Y. Tsivadze, *J. Porphyrins Phthalocyanines*, 2003, **07**, 795–800.
35 Y. Y. Enakieva, Y. G. Gorbunova, S. E. Nefedov and A. Y. Tsivadze, *Mendeleev Commun.*, 2004, **14**, 193–194.
36 L. A. Lapkina, Y. G. Gorbunova, S. E. Nefedov and A. Y. Tsivadze, *Russ. Chem. Bull.*, 2003, **52**, 1633–1636.
37 A. G. Martynov, O. V. Zubareva, Y. G. Gorbunova, S. G. Sakharov, S. E. Nefedov, F. M. Dolgushin and A. Y. Tsivadze, *Eur. J. Inorg. Chem.*, 2007, 4800–4807.
38 M. Capdevila-Cortada, J. Castelló and J. J. Novoa, *CrystEngComm*, 2014, 8232–8242.
39 M. Kasha, H. R. Rawls and M. A. El-Bayoumi, *Pure Appl. Chem.*, 1965, **11**, 371–392.
40 S. Yanagisawa, T. Yasuda, K. Inagaki, Y. Morikawa, K. Manseki and S. Yanagida, *J. Phys. Chem. A*, 2013, **117**, 11246–11253.
41 M. Sheik-Bahae, A. A. Said, T.-H. Wei, D. J. Hagan and E. W. Van Stryland, *IEEE J. Quantum Electron.*, 1990, **26**, 760–769.
42 R. L. Sutherland, *Handbook of Nonlinear Optics*, Marcel Dekker, New York, Marcel Dek., 1996.

